



## REVIEW

# Formation of Ag nanoparticles under electron beam irradiation: Atomistic origins from first-principles calculations

Juan Andrés<sup>1</sup>  | Amanda Fernandes Gouveia<sup>2</sup>  | Lourdes Gracia<sup>3</sup> |  
Elson Longo<sup>2</sup> | Giovani Manzeppi Faccin<sup>4</sup> | Edison Zacarias da Silva<sup>5</sup> |  
Douglas Henrique Pereira<sup>6,7</sup> | Miguel Angel San-Miguel<sup>6</sup>

<sup>1</sup>Department of Analytical and Physical Chemistry, University Jaume I, Castelló 12071, Spain

<sup>2</sup>Department of Chemistry, CDMF, Federal University of São Carlos, P.O. Box 676, São Carlos 13565-905, Brazil

<sup>3</sup>Department of Physical Chemistry, University of Valencia, Burjassot 46100, Spain

<sup>4</sup>Faculdade de Ciências Exatas e Tecnológicas, Universidade Federal da Grande Dourados, Unidade II, CP 533, 79804-970, Dourados, Mato Grosso do Sul, Brazil

<sup>5</sup>Department of Condensed Matter Physics, Institute of Physics 'Gleb Wataghin', State University of Campinas, 13083-970, Campinas, São Paulo, Brazil

<sup>6</sup>Department of Physical Chemistry, Institute of Chemistry, State University of Campinas, 13083-970, Campinas, São Paulo, Brazil

<sup>7</sup>Department of Biotechnology and Exact Sciences, Federal University of Tocantins, 77410-530, Gurupi, Tocantins, Brazil

## Correspondence

Juan Andrés, Department of Analytical and Physical Chemistry, University Jaume I, Castelló 12071, Spain.  
Email: andres@qfa.uji.es

## Funding information

Sistema de Computação Petaflopica SDUMONT-SINALAD-LNCC; National Center for High Performance Computing in São Paulo (CENAPAD); CCJDR-UNICAMP; FAPESP, Grant/Award Numbers: 2017/07240-8; 2013/26671-9, 2013/07296-2, 2015/19709-5; Capes and CNPq; Generalitat Valenciana (PrometeoII/2014/022, Prometeo/2016/079, ACOMP/2014/270, ACOMP/2015/1202); Ministerio de Economía y Competitividad, Grant/Award Number: CTQ2015-65207-P

## Abstract

The formation of Ag nanoparticles is currently a topic subject to a great deal of research because they are excellent materials with many technological applications. Recently, the formation of Ag nanoparticles on  $\alpha$ -Ag<sub>2</sub>WO<sub>4</sub> semiconductors induced by electron irradiation has been reported, but the mechanism underlying the transformations remains elusive. The aim of this article is to describe the mechanisms of electron beam irradiation on  $\alpha$ -Ag<sub>2</sub>WO<sub>4</sub> and its transformation to form Ag nanoparticles in vacuum conditions. To this end, a combined study involving experiments and multiscale computational approaches (density functional theory calculations and molecular dynamics simulations) is presented. With the increasing interplay between experimental and computational approaches at multiple length scales, we will also discuss how these combined data can be used to provide a deep insight into the rationalization of electron beam-induced transformations. This phenomenon is likely to be promoted by electron charge redistribution in these materials due to electronic excitations combined with the formation of silver vacancies under electron beam irradiation. As this mechanism should be relevant to other Ag-based materials, our results provide pointers for the further development and optimization of electron beam-mediated engineering of the atomic structure and electronic properties at the atomic resolution.

## KEYWORDS

$\alpha$ -Ag<sub>2</sub>WO<sub>4</sub>, Ag nanoparticles, electron beam irradiation, first-principles calculations, plasmons

## 1 | INTRODUCTION

In recent years, a strong continuous effort has been made in the synthesis of Ag nanoparticles (NPs) due to their remarkable properties and exciting applications in areas such as photonics, electronics, photocatalysis, sensing, and biomedicine.<sup>[1-12]</sup> The possibility of building new materials by

This article is dedicated to our colleague and friend, Prof. Nino Russo, as a tribute on the occasion of his 70th birthday. We hereby take this opportunity to convey our most heartfelt congratulations to an excellent person and a great researcher who possesses a privileged vision of interpersonal relations, teaching-learning processes, and technical-scientific innovations.

combining metallic Ag with a semiconductor gives rise to a broad spectrum of synergistic and complementary properties that enable new applications to be developed, and many studies have revealed that the deposition of Ag on semiconductors enhances their photocatalytic activity due to the particular properties of Ag-based photocatalysts.<sup>[13,14]</sup> This phenomenon is related to the surface plasmon resonance, which improves the separation of the electron-hole pair.<sup>[15–24]</sup> The controlled combination of these two different materials is an interesting challenge, in which Ag NPs on the contact interface trigger structural and electronic variations that affect the photocatalytic performance of the semiconductor by increasing the electron-hole separation and then the interfacial charge transfer processes, thereby contributing to improved photocatalytic activity.<sup>[25–28]</sup>

Our group is engaged in a research project devoted to the study of an unwanted real-time in situ process of nucleation and growth of Ag NPs on different silver-based semiconductors, which were driven by accelerated electron beam irradiation from an electron microscope under a high vacuum. In particular, under conditions that limit the dissipation of thermal energy and charge to a sufficient extent, the formation and growth of Ag NPs have been observed to occur in  $\alpha$ -Ag<sub>2</sub>WO<sub>4</sub> under in situ electron beam irradiation in SEM and TEM. The mechanisms underlying Ag NPs growth are still unknown and theoretical studies are contributing to gain insights into the atomistic processes involved.<sup>[29–33]</sup>

Silver tungstate,  $\alpha$ -Ag<sub>2</sub>WO<sub>4</sub>, is a material that has received special attention from the scientific community because of its applications in a variety of fields such as photoluminescence, bactericide behavior, gas sensor, and photocatalytic activity.<sup>[31,34–46]</sup>

The structural study of  $\alpha$ -Ag<sub>2</sub>WO<sub>4</sub> at the atomistic level using electron microscopy led to the discovery of a novel phenomenon that had not previously been reported in the literature: the electron irradiation on this material in electron microscopy leads to the formation of metallic Ag NPs.<sup>[30,36,47–49]</sup> However, along with the applications that have already been characterized, there is a strong interest in understanding the electron-semiconductor interactions leading to the formation of metallic silver on the surface of  $\alpha$ -Ag<sub>2</sub>WO<sub>4</sub> at a fundamental level.

Although this phenomenon seems to be conceptually simple, the underlying physics is complex and covers a broad range of time and length scales. Electron beam-matter interactions include a variety of physical and chemical effects with huge differences in the temporal and spatial scales, making comprehensive, first-principles modeling practically impossible. Thus, phenomena at very different time and length scales concur to establish the use of simplified models for aspects of the process and the observed data. At the nanoscale, the scenario is related to the making and breaking of chemical bonds and ultimately to the behavior of the electrons and their interactions with the material. Then, the possible elementary events and their interplay give rise to the mechanism.

A multiscale simulation would consider the electron interaction between the bulk material and the formation of Ag NPs, the diffusion processes of Ag NPs and their evolution. The ranges of applicability of the simulations can overlap, thereby opening up the possibility of mutual validation. To fulfil these requirements, in this article we will go over the path followed by our research programme to address this challenge. We will then provide an overview of the foundation and application of the hierarchical multiscale approach as a promising methodology for properly decoding the system complexity in first-principles modeling and analysis. The potential of the approach will be illustrated by means of a show-case in the context of unravelling the structural, thermodynamic and kinetic aspects of the nucleation and growth of Ag filaments from  $\alpha$ -Ag<sub>2</sub>WO<sub>4</sub> crystals on electron irradiation. Our calculations, based on computational methods within the framework of density functional theory (DFT) and ab initio molecular dynamic (MD) simulations, supply an atomistic approach to the local geometry and the electronic structure of the surfaces exposed to the electron beam irradiation. They also offer insights into the initial stages of the growth of metallic Ag on the  $\alpha$ -Ag<sub>2</sub>WO<sub>4</sub> surfaces when an electron beam is applied.

This manuscript provides a broad comprehensive overview of recent trends in which predictive modeling capabilities are developed in conjunction with experiments and advanced characterization to gain a greater insight into the formation of Ag NPs on  $\alpha$ -Ag<sub>2</sub>WO<sub>4</sub> and to study various physical-chemical phenomena and mechanisms. The focus of this review is on the intersections of multiscale materials experiments and modeling relevant to the materials community. How computational investigations are helpful to support, explain and provide an understanding of the experimental findings is also illustrated here. The article is organized as follows: the computational methodologies are discussed in section 3. In section 3.1, we study the electronic structure and behavior of  $\alpha$ -Ag<sub>2</sub>WO<sub>4</sub> when electrons are added. We then go on to investigate the impact of excess electrons to further analyse the Ag diffusion process as well as the formation of Ag nanowires and nanoparticles together with the nanoparticle interaction and coalescence events that occur under the TEM beam irradiation. Lastly, we conclude our study in Section 3.2. Thus, this fundamental work provides a new and important understanding of the formation and growth processes of Ag NPs on  $\alpha$ -Ag<sub>2</sub>WO<sub>4</sub>. The combination of experimental data and computational studies is a promising design strategy that has developed quickly over the past few years, allowing us to generate new materials with innovative properties, and should open up new opportunities for producing energy and chemicals from renewable resources.

## 2 | EXPERIMENTAL METHODS

### 2.1 | Synthesis

The synthesis route employed to obtain the  $\alpha$ -Ag<sub>2</sub>WO<sub>4</sub> crystals was described in great detail by Longo et al.<sup>[29,40]</sup> Initially, the precursors were prepared by separately dissolving  $1 \times 10^{-3}$  mol of tungstate sodium (Na<sub>2</sub>WO<sub>4</sub>·2H<sub>2</sub>O) and  $1 \times 10^{-3}$  mol of silver nitrate (AgNO<sub>3</sub>) in 50 mL of deionized water. Then, the  $\alpha$ -Ag<sub>2</sub>WO<sub>4</sub> nanostructures were obtained at 90°C by injecting the as-prepared precursors into hot aqueous solutions. The as-obtained suspensions were washed several times with deionized water to remove any remaining sodium ions.

## 2.2 | Characterization

The morphologies of  $\alpha$ -Ag<sub>2</sub>WO<sub>4</sub> crystals were examined using an Inspect F50 field-emission scanning electron microscope, FE-SEM (FEI Company, Hillsboro, OR) with an operating range of 5–15 kV. The electron dose used during all process was kept between 150 and 250 e/A<sup>2</sup>.s for the formation and nucleation process of Ag NPs on  $\alpha$ -Ag<sub>2</sub>WO<sub>4</sub> microcrystal, and the images were acquired in similar doses.

## 3 | COMPUTATIONAL METHODS AND MODELS

Our group employed two main computational methods. First of all, calculations of the electronic structure of crystals using DFT and ab initio molecular dynamics were employed to study the process of formation of Ag nanoclusters from  $\alpha$ -Ag<sub>2</sub>WO<sub>4</sub>.<sup>[33]</sup> These simulations spanned typical lengths of around 3 ps. The coalescence dynamics of the emerging silver nanoclusters, which in the experiments is mediated by resonance of surface plasmons, were then studied using classical molecular dynamics and empirical potentials.<sup>[50]</sup> Since this methodology is computationally less expensive, we were able to perform studies with a typical duration of 20 ns, which was enough to describe the crystallization dynamics of the system.

### 3.1 | $\alpha$ -Ag<sub>2</sub>WO<sub>4</sub> bulk

Theoretical calculation for the bulk  $\alpha$ -Ag<sub>2</sub>WO<sub>4</sub> structure was performed with a CRYSTAL14 program package.<sup>[51,52]</sup> The initial structure and the methodology are the same reposted by Longo et al.<sup>[47]</sup> The DFT associated with the B3LYP<sup>[53,54]</sup> functional hybrid were applied. Tungsten atom was described by a large-core ECP, derived by Hay and Wadt, and modified by Cora et al.<sup>[55]</sup> Silver and oxygen centers were described using HAYWSC-311d31G and O (6-31d1G) basis sets, respectively, which were taken from the Crystal Web site.<sup>[56]</sup> The diagonalization of the Fock matrix was performed at adequate *k*-points grids in the reciprocal space. The thresholds controlling the accuracy of the calculation of the Coulomb and exchange integrals were set to 10<sup>-8</sup> (ITOL1 to ITOL4) and 10<sup>-14</sup> (ITOL5), and the percent of Fock/Kohn-Sham matrices mixing was set to 40.<sup>[51]</sup> The density of states (DOS) projected on atoms and orbitals of  $\alpha$ -Ag<sub>2</sub>WO<sub>4</sub> were constructed along the appropriate high-symmetry directions of the corresponding irreducible Brillouin zone.

### 3.2 | Diffusion processes

These calculations were performed within the framework of DFT as implemented in the VASP package.<sup>[57-59]</sup> An energy cutoff of 460 eV was adopted, corresponding to a convergence of at least 1 meV/atom. Brillouin zone integrations were made using converged Monkhorst-Pack grids<sup>[60]</sup> and also the tetrahedron method with Blöchl corrections.<sup>[61]</sup> We chose to use the PBE approximation for the exchange and correlation<sup>[62,63]</sup> and the PAW method to handle core electrons.<sup>[64,65]</sup> The valence states that were explicitly included in the calculation were 4d and 5s (11 electrons) for Ag atoms, 5d and 6s (6 electrons) for W atoms, and 2s and 2p (6 electrons) for O atoms. Forces were evaluated through the Hellmann-Feynman theorem<sup>[66]</sup> and the structures were relaxed until the forces were less than 0.005 eV Å per atom. The simulated models did not consider spin-polarization effects. The study of the diffusion process of Ag in the system was investigated using the nudged elastic band (NEB) method.<sup>[67]</sup> In the NEB method the initial and final configurations were previously optimized. The intermediate configurations were generated by linear interpolation between initial and final points and all intermediate were relaxed following a NEB methodology.<sup>[67]</sup> To perform the addition of electrons in the bulk  $\alpha$ -Ag<sub>2</sub>WO<sub>4</sub> structure the keyword NELECT was used, and all the crystal structures were optimized simultaneously for both the volume of the unit-cell and atomic positions. The relationship between the charge density topology and elements of molecular structure and bonding was reported by Bader and others.<sup>[68,69]</sup> This relationship can be analyzed using the quantum theory of atoms in molecules (QTAIM).<sup>[68,70,71]</sup> This QTAIM is now a well-recognized tool used to analyze electron density, describe interatomic interactions, and rationalize chemical bonding.<sup>[72]</sup> This approach is well-known and is described in several papers in the literature.<sup>[30,73,74]</sup>

### 3.3 | Classical molecular dynamics methods

The study of crystallization dynamics of Ag NPs requires simulations that are longer in time and thus computationally too expensive for ab initio methods. To study this aspect of the phenomena we have employed molecular dynamics (MD) simulations using the LAMMPS package,<sup>[75-78]</sup> in which models for Ag NPs designed to be similar to the real NPs from the experiments are coalesced under different temperature setups. To perform such simulations, the canonical ensemble (NVT) was simulated using Nosé-Hoover thermostat chains,<sup>[79-81]</sup> using small timesteps of 1 fs for the integration of the equations of motion so that negligible numerical deviations would occur in the atomic trajectories during the simulations. To describe the interaction between atoms we have used the embedded atom model (EAM)<sup>[82-85]</sup> with the parametrization for Ag from Sheng et al.,<sup>[86]</sup> which was optimized to reproduce the mechanical properties of silver, including the cohesive energy, lattice constant, bulk modulus, elastic constants, phonon dispersion curves, dilatation behavior, melting temperature, and energy differences between different crystalline phases, thus providing a mechanical description of Ag NPs that is the closest possible to DFT in this size and time scales. Finally, it's important to mention the packages used for the creation of images and movies, which were VMD and Ovito<sup>[87-89]</sup> and the common neighbor analysis (CNA) of Dana et al.<sup>[90]</sup>

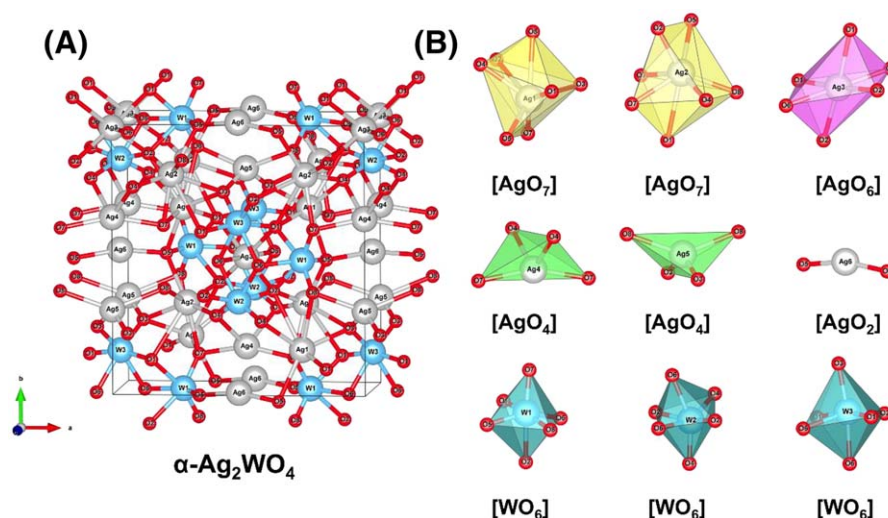


FIGURE 1 Orthonorhombic structure of  $\alpha\text{-Ag}_2\text{WO}_4$ . A, Bulk, B,  $[\text{AgO}_n]$  with  $n = 7, 6, 4$ , and  $2$ , and  $[\text{WO}_6]$  clusters

## 4 | RESULTS AND DISCUSSION

### 4.1 | Analysis of $\alpha\text{-Ag}_2\text{WO}_4$ bulk

The properties obtained by  $\alpha\text{-Ag}_2\text{WO}_4$  can be attributed to the flexibility of its geometric structure, in which the Ag cations adopt different local coordination sites.<sup>[29,40,91]</sup> Figure 1 shows the orthonorhombic structure of  $\alpha\text{-Ag}_2\text{WO}_4$ .

The  $\alpha\text{-Ag}_2\text{WO}_4$  structure was resolved by our research group<sup>[40]</sup> and is composed of octahedral  $[\text{WO}_6]$  and  $[\text{AgO}_n]$  clusters ( $n = 7$ , deltahedral  $[\text{AgO}_7]$ ;  $n = 6$ , octahedral  $[\text{AgO}_6]$ ;  $n = 4$ , tetrahedral  $[\text{AgO}_4]$ ; and  $n = 2$ , angular  $[\text{AgO}_2]$ ) as depicted in Figure 1. Due to its particular geometry, structural and electronic distortions take place and then variations in Ag—O and W—O bond lengths and O—W—O and O—Ag—O angles are sensed.<sup>[29,30]</sup> The properties of this semiconductor change according to the crystallographic phase, size, and morphology, and these variables are all dependent on the synthesis procedure. Each surface of a crystal can possess a particular surface energy, atomic distribution, local coordination (clusters) of exposed metals, vacancies, and so on. Finding the method of synthesis that allows these characteristics to be controlled is crucial to be able to exploit their properties and subsequent technological applications.

Figure 2 shows the partial DOS projected on Ag, W, and O orbitals and the total DOS projected over all the atoms in the  $\alpha\text{-Ag}_2\text{WO}_4$  structure.

The analysis of the total DOS in Figure 2D shows that the valence band (VB) is predominantly composed of O atoms and Ag atoms, while the conduction band (CB) is mainly formed by W atoms with a minor contribution of Ag atoms. The atomic orbitals in the VB from O atoms are  $p$ -type ( $2p_x + 2p_y + 2p_z$  and  $3p_x + 3p_y + 3p_z$ ) orbitals, while in the case of the Ag atoms they are  $d$ -type ( $4d_{xz} + 4d_{yz} + 4d_{xy}$  and  $4d_{z^2} + 4d_{x^2-y^2}$ ) orbitals. In the CB, the orbitals are  $d$ -type ( $5d_{xz} + 5d_{yz} + 5d_{xy}$  and  $5d_{z^2} + 5d_{x^2-y^2}$ ) and  $s$ -type ( $6s$ ) orbitals from W atoms and Ag atoms, respectively.

The partial DOS in Figure 2A–C for Ag atoms, W atoms, and O atoms, respectively, shows that at the top of the VB is derived from  $2p_z$  orbitals and  $4d_{z^2} + 4d_{xz}$  orbitals from O and Ag atoms, respectively. These atomic orbitals between the O and Ag orbitals are of the bonding orbitals type. For the bottom of the CB there are  $5d_{x^2-y^2}$  orbitals and  $4s$  orbitals from W and Ag atoms, respectively. The orbitals in the CB are mainly of the bonding orbitals type, formed by hybridization of Ag  $6s$ , O  $2p$ , and W  $5d$  orbitals.

### 4.2 | Formation of Ag NPs on $\alpha\text{-Ag}_2\text{WO}_4$ crystals

The nucleation and growth of Ag NPs are initiated by irradiating the  $\alpha\text{-Ag}_2\text{WO}_4$  with the electron beam. Figure 3 presents typical images of this event in real-time using FE-SEM spectroscopic techniques. A burst of nucleation is observed when the sample is focused for imaging, followed by the continuous appearance of new Ag NPs. Although nanoparticle coalescence events occur in the early stage of growth, most nanoparticles eventually develop into isotropic nanostructures via the attachment of monomeric species.<sup>[48]</sup>

### 4.3 | Earlier stages in Ag diffusion

The nucleation and growth of metallic Ag in  $\alpha\text{-Ag}_2\text{WO}_4$  crystals when irradiated by electron beams is initiated in the surface. The most superficial Ag atoms probably diffuse outwards creating surface vacancies, which aid other diffusion processes from inner lattice positions. Simultaneously, the initial  $n$ -type semiconductor system is converted an  $p$ -type semiconductor. The formation of metallic structures as a result of irradiating them with

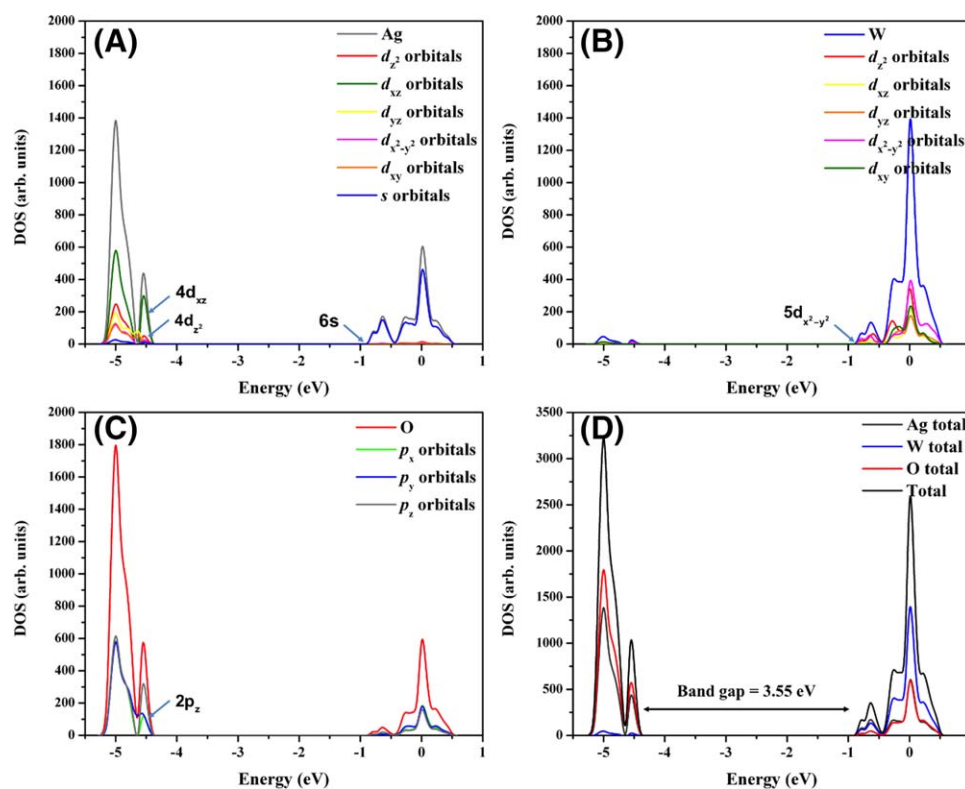


FIGURE 2 Partial DOS projected on: A, Ag orbitals, B, W orbitals, and C, O orbitals; and D, Total DOS projected in  $\alpha$ - $\text{Ag}_2\text{WO}_4$  structure

SEM and TEM leaves the material in a crystalline state as has been observed with X diffraction techniques.<sup>[29]</sup> This system is different from other materials in which a disordering process leading to amorphous regions occurs on electron irradiation.<sup>[92–96]</sup>

We intend to analyze this phenomenon by exploring all possible diffusion routes for the most superficial Ag atoms in two exhibited surfaces: the (100) and the (001) surfaces, see Figure 4A,B.

It is worth noticing that the (001) surface reveals a modified arrangement that is very different from the ideal cleavage due to the stabilization of the external polyhedral clusters. This surface can be understood as an assembly of corner-sharing Ag polyhedra, as shown in Figure 4C, in which

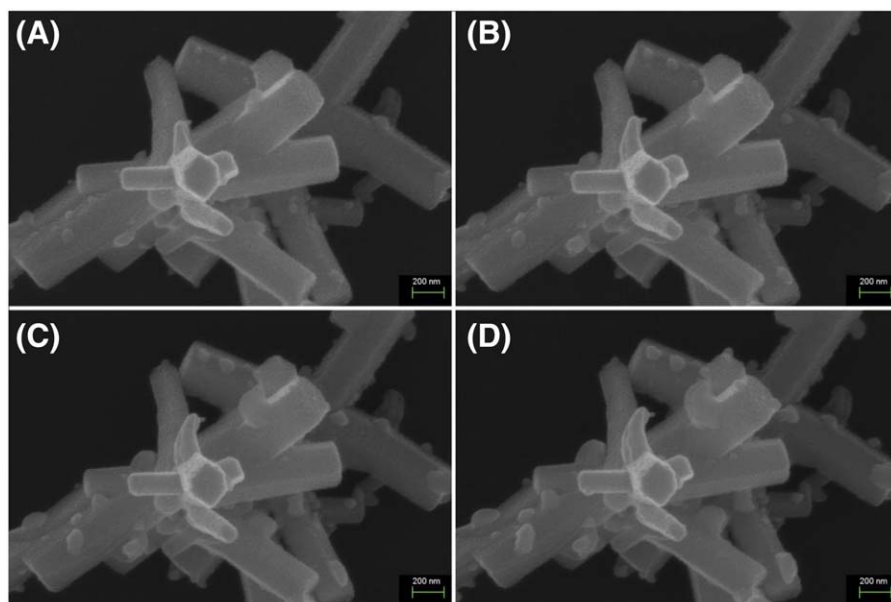
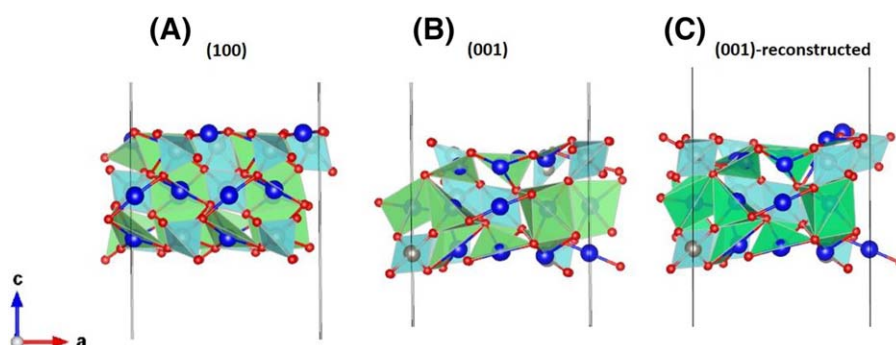


FIGURE 3 FEM-SEM images of the growth evolution of Ag NPs on  $\alpha$ - $\text{Ag}_2\text{WO}_4$  crystal with time: A,  $t = 0$  min, B,  $t = 3$  min, C,  $t = 6$  min, and (D)  $t = 9$  min



**FIGURE 4** The three-layers model for  $\alpha$ - $\text{Ag}_2\text{WO}_4$  surfaces: A, (100), B, (001), and C, (001)-reconstructed. Ag, W, and O atoms are colored in blue, gray, and red, respectively

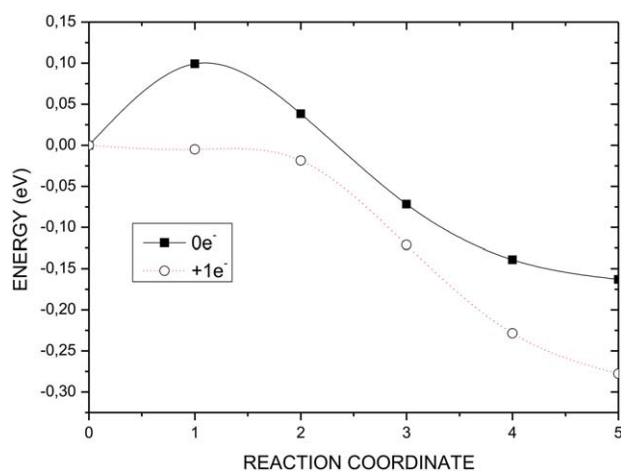
external effects such as pressure and temperature fluctuations or the influence of different solvents involving molecular adsorption processes might modify—even significantly—the arrangement of these polyhedra and consequently the surface stability. Table 1 shows the coordination numbers (CNs) for all the Ag atoms in the three surfaces: (100), (001), and (001)-reconstructed. Their CNs range from 2 to 6, thereby indicating that the surface Ag atoms are in quite different polyhedral environments. The initial idea is to try to correlate the ability to diffuse to specific CNs (i.e., type of cluster). Thus, all cases of surface Ag polyhedra were studied. Our approach was to use the NEB method to estimate the energy barrier for each Ag atom in each surface cluster to move outside. First and prior to the NEB calculations, to study the stability of Ag atoms in their final position outside the surface, we performed calculations of geometry optimization after displacing one Ag atom to a position outside the surface. It was found that only specific Ag atoms in each surface are able to diffuse, whereas there are other atoms that remain in the original position. Table 1 shows all the most superficial Ag atoms in the supercell studied. The energy barriers calculated using this method are reported for atoms that are potentially diffusive. It can be seen that all computed barriers are smaller than 0.1 eV, and they are not related to one kind of CN. This means that the Ag atoms can diffuse from different cluster structures with CN of 3, 4, and 6.

Figure 5 shows the energy profile for the diffusion process of Ag-3 in the (001) surface before being irradiated by the electron beam. It can be seen that the diffusion pathway from the initial structure to the final one involves an energy barrier of about 0.10 eV. This energy value is relatively low, suggesting this Ag surface atom as a good candidate for initiating the diffusion process. The energy profiles for all the other Ag atoms can be seen in the Supporting Information (Figures SI-2-SI-6). They show similar energy barriers although the curve habits are different.

One of the effects that the electron bombardment occurring during the TEM experiments might produce is electron injection. Our intention was to investigate the structural and electronic consequences of the system absorbing density charge from the electron beam. In fact, simulating the introduction of excess electrons in the computational cell shows significant alterations even at low rates. Figure 5 also illustrates the energy profile for the diffusion of Ag-3 in the (100) surface for a ratio of just  $1 \text{ e}^-/\text{cell}$ . It becomes evident that the initially estimated energy barrier of 0.10 eV vanishes (dotted line). The electron injection also promotes structural modifications in the local Ag arrangements. This effect is exemplified in Figure 6, which displays the (100) surface before and after injecting  $5 \text{ e}^-/\text{cell}$ . The structures for the lower rates are also shown in the Supporting Information (Figure SI-1). It is clear that the absorption of electrons involves structural rearrangements particularly in the local Ag-3 environment. The Ag atom moves upwards as the number of electrons increases, and the neighboring O atoms are also displaced appreciably.

**TABLE 1** Coordination numbers (CN) and estimated energy barriers ( $\Delta E$ , in eV) for all Ag atoms in the (100), (001), and (001)-reconstructed surfaces

Atom	(100)		(001)		(001)-reconstructed	
	CN	$\Delta E$	CN	$\Delta E$	CN	$\Delta E$
Ag-1	4	-	6	-	5	-
Ag-2	4	-	6	-	6	-
Ag-3	4	0.1	4	-	4	-
Ag-4	4	0.1	3	0.03	4	0.08
Ag-5	6	-	3	0.03	3	0.05
Ag-6	6	-	4	-	3	-
Ag-7	6	0.1	5	-	2	-
Ag-8	6	0.1	5	-	3	-



**FIGURE 5** Energy profiles for the diffusion process of the Ag-3 atom in the (100) surface in a neutral system (black line) and when one electron is added into the system (dot line). Reproduced from Ref. [32] with permission from the PCCP Owner Societies

The analysis of the density distribution in the system along the diffusion process of the Ag atom has been performed using the Bader charges. Figure 7 shows those values for the Ag-3 diffusion processes before and after  $1 e^-$ /cell injection. In the neutral system a reduction occurs (since the Ag atom in the final structure has a higher Bader charge value) while, in contrast, for the system with 1 injected electron the Ag atom is oxidized. It is worth noticing that both the charge gain and the charge loss do not occur linearly along the diffusion pathway. The local values for each image along the process fluctuate notably for short displacements. These facts suggest that complex processes of electron density redistribution occur during the atom diffusion involving numerous neighboring atoms.

As has been illustrated in this section and as a tentative conclusion, the initial metallic Ag nucleation process might be initiated by specific superficial Ag atoms, which are able to diffuse outwards with low energy barriers that are also reduced by the charge injection induced by the electron beam. This phenomenon is also accompanied by order-disorder effects that alter the electronic properties as seen from the charge density fluctuations along the diffusion pathway, but which simultaneously preserve other crystalline regions, as confirmed by the experimental evidence.

#### 4.4 | Electron addition in $\alpha$ -Ag<sub>2</sub>WO<sub>4</sub>

Quantum mechanical calculations were performed to understand the real-time in situ nucleation and growth of Ag filaments on  $\alpha$ -Ag<sub>2</sub>WO<sub>4</sub> crystals observed experimentally.<sup>[29,30]</sup> An analysis and a comparison of the geometries for neutral ( $N = 0$ ) and charged ( $N = 10$ ) structures shows a pronounced increase in the corresponding Ag–O distances with the addition of electrons. In the [AgO<sub>2</sub>] cluster, the Ag–O distance increases from 2.15 to 2.81 Å. In the [AgO<sub>4</sub>] cluster, two different distances are observed: one pair exhibits a similar behavior to that of the bonds in the [AgO<sub>2</sub>] cluster and has an O–Ag–O angle of approximately 170°; the other pair has an O–Ag–O angle of approximately 108° and a longer Ag–O distance, which indicates that the atoms detach as the electrons are added. In fact, when  $N = 10$ , the first pair of O atoms form an O–Ag–O angle of approximately 178°, whereas the angle of the second pair is reduced to approximately 90°, as shown in Figure 8.

In the two types of [WO<sub>6</sub>] clusters, we find that the W–O distances corresponding to the W2 and W3 atoms remain almost unaltered, whereas the distance of the W–O bond corresponding to W1 decreases smoothly with the addition of electrons. These results show that during electron

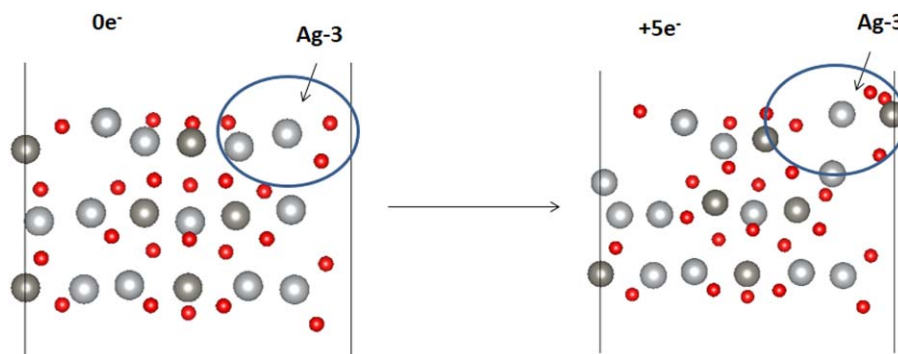


**FIGURE 6** Structural representation of Ag atoms in the  $\alpha$ -Ag<sub>2</sub>WO<sub>4</sub> (100) surface along z-axis before and after injecting  $5 e^-$ /cell. Previous charge additions at lower taxes can be seen in the Supporting Information

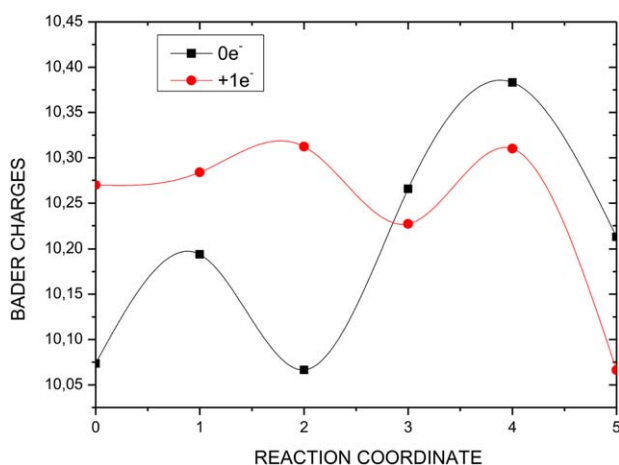


**FIGURE 7** Bader charges for the diffusion process of the Ag-3 atom in the (100) surface without (black line) and with 1 e<sup>-</sup>/cell addition (red line)

irradiation, electronic and structural disorder was introduced into the material, thus illustrating the fundamental role of cluster concepts in the formation and growth of Ag filaments.

Finding zero flux surfaces between two atoms allows the charge of each atom to be calculated. In Table 2, the charge density of the Ag and W centers of the [AgO<sub>2</sub>], [AgO<sub>4</sub>], and [WO<sub>6</sub>] clusters is presented as a function of the number of electrons added. Atomic charges were calculated by using integrations of the charge density of the atomic basins,  $\Omega$ , and subtracting the nuclear charge,  $Z$ , of the corresponding atom as follows.

$$q(W) = ZW - N(W) \text{ with } N(\Omega) = \int_{\Omega} \rho(\Omega) dr$$

In addition, the average bond distances of Ag4–Ag5 as a function of the number of electrons added are shown in Table 1.

An analysis of the results presented in Table 1 reveals that the Ag<sub>6</sub> atoms of the [AgO<sub>2</sub>] clusters are the atoms most prone to reduction. At  $N = 7$ , the Ag<sub>6</sub> atoms are practically reduced, whereas the Ag<sub>4</sub>/Ag<sub>5</sub> centers require at least 10 electrons to reach the same state. This behavior implies the existence of two different paths to obtain metallic Ag, which are associated with the [AgO<sub>2</sub>] and [AgO<sub>4</sub>] clusters. In the case of W atoms that form [WO<sub>6</sub>] clusters, W1 atoms behave differently to W2 and W3 atoms, and a minor decrease in electron density relative to that of the Ag centers is observed (a decrease of 0.2 units at  $N = 10$ ). Therefore, the extra electron density added to the material is transferred from one cluster to another through the lattice network, and the Ag-formation process involves both adjacent [AgO<sub>2</sub>] and [AgO<sub>4</sub>] clusters and, to a minor extent, [WO<sub>6</sub>] clusters. During electron irradiation, electronic and structural disorder is introduced into the material, thereby indicating the fundamental role that cluster concepts play in the formation and growth of Ag filaments.

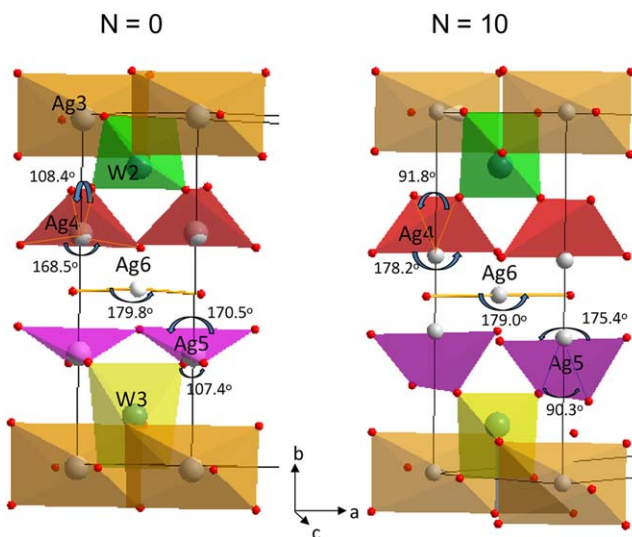


**FIGURE 8** Geometry of neutral ( $N = 0$ ) and charged ( $N = 10$ ) structures, focused on distances and angle variations on [AgO<sub>2</sub>] and [AgO<sub>4</sub>] clusters



**TABLE 2** Charge density of the Ag and W centers in [AgO<sub>2</sub>], [AgO<sub>4</sub>], and [WO<sub>6</sub>] clusters, and average Ag<sub>4</sub>–Ag<sub>5</sub> distances (in Å) as a function of the number of electrons added

N e	[WO <sub>6</sub> ] (W1)	[AgO <sub>4</sub> ] (Ag4/Ag5)	[AgO <sub>2</sub> ] (Ag6)	Ag <sub>4</sub> –Ag <sub>5</sub>
0	2.818	0.653	0.665	3.36
1	2.794	0.596	0.566	3.00
2	2.772	0.526	0.453	2.92
3	2.700	0.425	0.331	2.83
4	2.679	0.354	0.204	2.75
5	2.611	0.233	0.086	2.68
6	2.584	0.196	0.060	2.71
7	2.545	0.176	0.032	2.70
8	2.508	0.100	−0.119	2.66
9	2.476	0.072	−0.143	2.67
10	2.455	0.069	−0.159	2.67

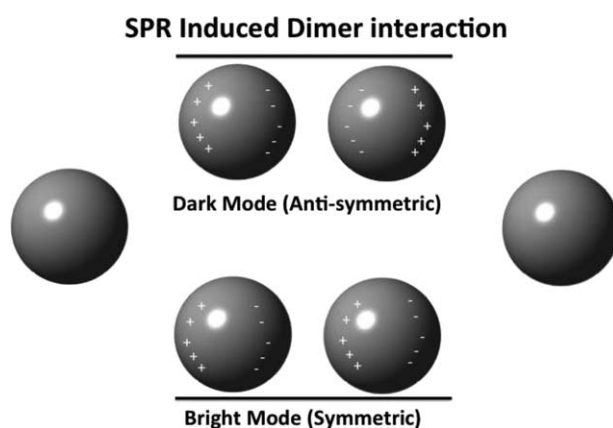
$q(\Omega)$  represents the number of valence electrons minus the calculated charge density.

#### 4.5 | Coalescence of Ag NPs

The discussion of the formation of Ag clusters and coalescence events is motivated by the recent observation of a complex process involving the formation and subsequent growth of Ag nanocrystals through an unexpected additive-free in situ fabrication process and crystal growth mechanism under electron beam irradiation.<sup>[48]</sup> That work showed that the TEM electron beam, as well as producing Ag nanowires, also produces free Ag clusters in vacuum. They further observed that nearby clusters interacted, sometimes attracting and at other times repelling each other. We recently used computer simulations<sup>[50]</sup> to show that these attractive processes leading to coalescence events can be explained. The mechanism with a physics-based description underlying the unusual in situ Ag NPs coalescence was explained as a result of surface plasma resonances (SPR) and their interaction. Experiments showed images of the temporal evolution of the Ag NPs and their interactions forming other larger Ag NPs. SPR, understood from Mie theory and neutral dipole interactions, are used to explain the observed effect. To this end, and as a valuable complement to such experimental observations, a comprehensive study has been carried out by using MD simulation methods to provide insights into the structural changes, energetics and electronic properties of the Ag NPs, which are hardly available from the experimental methods.

The main idea accounting for this new observed effect can be explained with the help of Figure 9. Previous studies of metal NPs have shown that, similarly to the case of laser irradiation, electron beam irradiation also produces electromagnetic wave radiation (EWR) that acts on the NPs. Ag NPs are wavelength (or frequency) filters for this EWR and the resonance results in SPR neutral objects. These SPR behave as nanoelectric dipoles, whose interaction process can be understood from Figure 9.

Using Mie theory as their basis, Koh et al.<sup>[97]</sup> have shown that two nearby NPs in the SPR states can form bonding and antibonding states. Our reasoning is that when two NPs are in the bonding state the dipole–dipole interaction will cause mutual attraction, which will consequently lead to a

**FIGURE 9** Dimer interaction mechanism. SPR in the Ag NPs induces neutral dipole-dipole interactions causing dimer attraction in the symmetric dimer mode

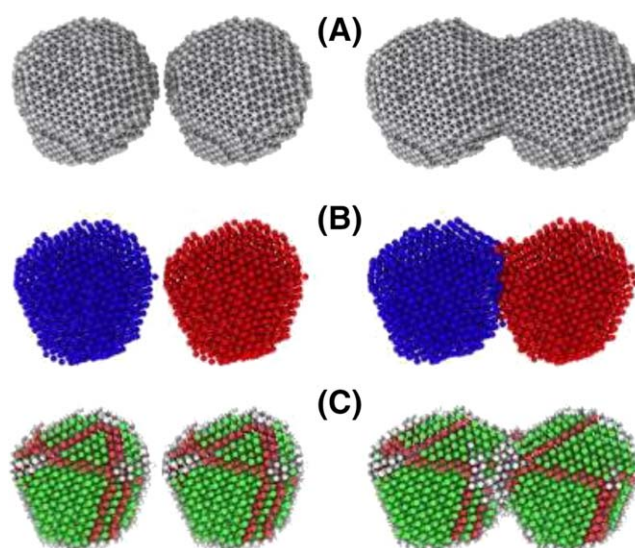


**FIGURE 10** A, MD snapshots of two Ag NPs before and after coalescence attachment, B, Color coded NPs, and C, Common neighbor analysis (CNA) of the same structures

coalescence process. To further pursue these ideas, we considered computer simulations of nearby NPs and followed their dynamical evolution. A typical example of these computer simulations is shown in Figure 10; (a) shows the initial and advanced stages of the coalescence process; and (b) provides the same snapshots using a color-coded filter for the atoms along with a filter that slices the NPs in half, thus allowing visualization of their interior. The color code is blue for atoms originally from one NP and red for atoms originally from the other NP, which makes it easier to follow the diffusion of particles during the coalescence process. To further understand the evolution process, in (c) the common neighbor analysis (CNA) method has been employed to evidence the local atomic environment and displays face-centered cubic (fcc) ordered regions (green), hexagonal close-packed (hcp) stacking faults (red), or disordered local environments (gray), together with the same slice filter. Using these forms of analysis we will detail our findings by describing the simulations that can be associated to the experimental steps to understand coalescence and sintering of Ag NPs.

The simulations presented here are similar to those we presented previously in another study.<sup>[50]</sup> In this case, we considered the coalescence of two NPs with sizes of 4.3 and 6.0 nm, which could represent a typical experimental coalescence event. Simulations were performed at temperatures of 500 K and 900 K, here, we will discuss only the 900 K results since temperature effects help the evolution of the coalescence and are more

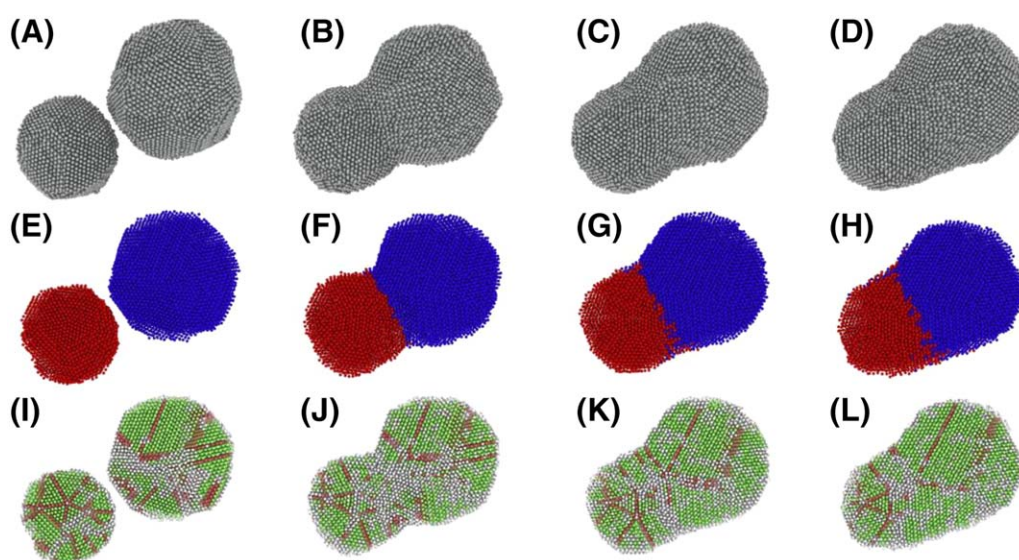


**FIGURE 11** Simulation of the coalescence of a 4.3 nm NP with a 6.0 nm NP at 900 K. A-D, structural evolution of the coalescence; E-H, plane cut with atoms color coded for each initial NP; G-K, the CNA plots that depict how the structure evolves from disordered to partially fcc ordered regions (green) with hcp (red) defects/stacking faults

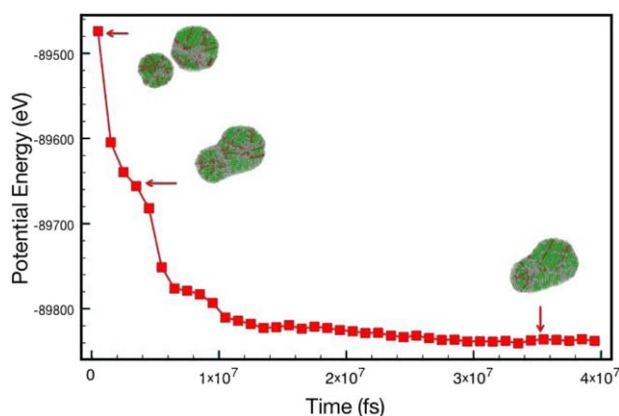


**FIGURE 12** Energy profile of the coalescence simulation of a 4.3 nm Ag NP with a 6.0 nm Ag NP at 900 K, shown in Figure 11

appropriate to explain the experimental coalescence process. The reason why we consider this temperature is that the SPR in the NPs are accompanied by energy absorption, which increases the temperature of the NPs taking them close to their melting transition.

Figure 11 shows selected snapshots of the coalescence process at 900 K. Figure 11A shows the two NPs before contact, Figure 11E shows a planar cut of the NPs with color coding for each NP, Figure 11I offers the CNA analysis depicting ordered fcc (green atoms) regions, hcp (red atoms) defects and disordered regions (gray atoms). We believe that such NPs closely represent the experimentally produced Ag NPs seen in the experiments. Figure 11A–D display the evolution of the NPs coalescence in the formation of a new NP, showing the evolution of the neck interface along with the faceting of the structure. Figure 11E–H show a planar cut of the same structures with color coding of the atoms, which helps to understand the atom diffusion: blue atoms can be seen diffusing into the red atom region as well as the opposite, namely, red atoms diffusing into the blue region. It can be observed that there is also a small surface diffusion. Figure 11I–L presents the CNA analysis, where it is possible to follow the evolution of the order during the process. The two NPs (Figure 11I) have stacking faults, disordered regions and some ordered fcc regions. The coalescence process starts with the neck formation which shows that on touching, a disordered interface forms at the neck region (Figure 11J). As the evolution continues, at  $t = 8.5$  ns (Figure 11K) healing towards the formation of ordered interface continues and the number of stacking faults is also reduced. Figure 11L shows the final image at 35 ns of the new NP further ordered with small disordered regions and few stacking faults. During the MD simulation the average potential energy (APE) of the system was monitored and the calculation was stopped when the APE stabilized at a lower energy plateau, as can be seen in Figure 12.

The surprising results of coalescence were a bonus feature in addition to the already interesting and novel behavior presented by  $\alpha$ - $\text{Ag}_2\text{WO}_4$  when irradiated by the electron beam in the experiments. Our theoretical reasoning, helped by MD computer simulations, added to the understanding of these interesting events. Further experiments and simulations are under way to further explore them.

## 5 | CONCLUSIONS

The recent advances in electron–matter studies have opened up new experimental possibilities to manipulate materials at the atomic scale. In particular, FE-SEM and TEM are very powerful methods that can address a multitude of investigative challenges and can be used not only to offer a spectroscopic technique to identify surface facets, morphology, and defects in the crystal, but also to do so on an atomic scale. This technique yielded valuable insights into the material investigated under the effects of an electron beam, where high-energy electrons are transmitted through the specimen, while also providing useful microstructure and electronic structure information about the samples based on electron–solid interaction. Because of the bombardment of high-energy electrons, some novel phenomena have been discovered to illustrate the potential of FE-SEM and TEM. Moreover, first-principles calculations, simulations and modeling are fundamental to rationalize the properties of materials in both basic and applied research. New research directions are emerging in materials science by increasing the interplay between experimental results and computational approaches. Such cooperative interactions find many applications by providing a deeper insight in the properties and phenomena in complex material systems.

Here, we present the experimental techniques and computational and theoretical methods and procedures our group uses to investigate the formation of Ag NPs on  $\alpha$ - $\text{Ag}_2\text{WO}_4$  semiconductor under electron beam irradiation. Our results not only shed light on the underlying mechanism, at the atomic level but also account for the variations in structural and electronic properties.

The mechanism that we discussed provides pointers for further developments and optimization of perhaps the most intriguing aspects of 3D material engineering using an electron beam, as seamless nanoscale modification of the fundamental physical properties is possible for device and circuit design with unparalleled combinations of miniaturization and integration.

The possibilities are numerous, and because the formation of Ag NPs can be extended to other Ag-based materials, understanding of the mechanisms involved is essential to develop rational routes to such extreme material modification using scalable techniques, such as high-brightness electron beam lithography. Hence, the envisioned extension of the hierarchical multiscale approach to the description of this behavior will constitute a relevant change of paradigm in the analysis and design of complex phenomena, paving the way towards rational development based on functional understanding rather than empirical testing.

## ACKNOWLEDGMENTS

The simulations were performed at the Sistema de Computação Petaflopica SDUMONT-SINAPAD-LNCC, the National Center for High Performance Computing in São Paulo (CENAPAD) and at the CCJDR-UNICAMP. We acknowledge support from FAPESP (2017/07240-8; 2013/26671-9, 2013/07296-2, 2015/19709-5). Partial support was provided by Capes and CNPq. J.A. acknowledges the financial support of agencies: Generalitat Valenciana for PrometeoII/2014/022, Prometeo/2016/079, ACOMP/2014/270, ACOMP/2015/1202, Ministerio de Economía y Competitividad, project CTQ2015-65207-P.

## ORCID

Juan Andres  <https://orcid.org/0000-0003-2656-5811>

Amanda Fernandes Gouveia  <http://orcid.org/0000-0003-3441-3674>

## REFERENCES

- [1] R. C. Jin, Y. W. Cao, C. A. Mirkin, K. L. Kelly, G. C. Schatz, J. G. Zheng *Science* **2001**, 294, 1901.
- [2] Y. Sun, Y. Xia, *Science* **2002**, 298, 2176.
- [3] E. Braun, Y. Eichen, U. Sivan, G. Ben-Yoseph, *Nature* **1998**, 391, 775.
- [4] B. J. Wiley, S. H. Im, Z. Y. Li, J. McLellan, A. Siekkinen, Y. N. Xia, *J. Phys. Chem. B* **2006**, 110, 15666.
- [5] J. M. Sun, D. Ma, H. Zhang, X. M. Liu, X. W. Han, X. H. Bao, G. Weinberg, N. Pfander, D. S. Su, *J. Am. Chem. Soc.* **2006**, 128, 15756.
- [6] A. Tao, F. Kim, C. Hess, J. Goldberger, R. R. He, Y. G. Sun, Y. N. Xia, P. D. Yang, *Nano Lett.* **2003**, 3, 1229.
- [7] C. Gunawan, W. Y. Teoh, C. P. Marquis, J. Liffa, R. Amal, *Small* **2009**, 5, 341.
- [8] H. Fang, Y. Wu, J. H. Zhao, J. Zhu, *Nanotechnology* **2006**, 17, 3768.
- [9] A. D. McFarland, R. P. Van Duyne, *Nano Lett.* **2003**, 3, 1057.
- [10] T. Thiwawong, K. Onlaor, B. Tunhoo, *Adv. Mater. Sci. Eng.* **2013**, 2013, 640428.
- [11] J. Kahler, A. Stranz, A. Waag, E. Peiner, *J. Electron. Mater.* **2014**, 43, 2397.
- [12] P. Peng, A. M. Hu, A. P. Gerlich, G. S. Zou, L. Liu, Y. N. Zhou, *Acs Appl. Mater. Interfaces* **2015**, 7, 12597.
- [13] Z. G. Yi, J. H. Ye, N. Kikugawa, T. Kako, S. X. Ouyang, H. Stuart-Williams, H. Yang, J. Y. Cao, W. J. Luo, Z. S. Li, Y. Liu, R. L. Withers, *Nat. Mater.* **2010**, 9, 559.
- [14] J. D. Li, W. Fang, C. L. Yu, W. Q. Zhou, L. H. Zhu, Y. Xie, *Appl. Surf. Sci.* **2015**, 358, 46.
- [15] Y. J. Luo, X. M. Liu, X. H. Tang, Y. Luo, Q. Y. Zeng, X. L. Deng, S. L. Ding, Y. Q. Sun, *J. Mater. Chem. A* **2014**, 2, 14927.
- [16] C. L. Yu, L. F. Wei, X. Li, J. C. Chen, Q. Z. Fan, J. C. Yu, *Mater. Sci. Eng. B Adv. Funct. Solid State Mater.* **2013**, 178, 344.
- [17] S. Linic, P. Christopher, D. B. Ingram, *Nat. Mater.* **2011**, 10, 911.
- [18] G. Baffou, R. Quidant, *Chem. Soc. Rev.* **2014**, 43, 3898.
- [19] P. Christopher, H. L. Xin, S. Linic, *Nat. Chem.* **2011**, 3, 467.
- [20] Y. Q. Liang, Z. D. Cui, S. L. Zhu, Y. Liu, X. J. Yang, *J. Catal.* **2011**, 278, 276.
- [21] T. Zidki, R. Bar-Ziv, U. Green, H. Cohen, D. Meisel, D. Meyerstein, *Phys. Chem. Chem. Phys.* **2014**, 16, 15422.
- [22] M. Y. Zhu, C. J. Wang, D. H. Meng, G. W. Diao, *J. Mater. Chem. A* **2013**, 1, 2118.
- [23] C. M. Cobley, S. E. Skrabalak, D. J. Campbell, Y. N. Xia, *Plasmonics* **2009**, 4, 171.
- [24] H. R. Tan, R. Santbergen, A. H. M. Smets, M. Zeman, *Nano Lett.* **2012**, 12, 4070.
- [25] Y. P. Bi, S. X. Ouyang, J. Y. Cao, J. H. Ye, *Phys. Chem. Chem. Phys.* **2011**, 13, 10071.
- [26] H. Y. Hu, Z. B. Jiao, T. Wang, J. H. Ye, G. X. Lu, Y. P. Bi, *J. Mater. Chem. A* **2013**, 1, 10612.
- [27] Y. P. Bi, H. Y. Hu, S. X. Ouyang, Z. B. Jiao, G. X. Lu, J. H. Ye, *Chemistry* **2012**, 18, 14272.
- [28] T. J. Yan, W. F. Guan, Y. Xiao, J. Tian, Z. Qiao, H. S. Zhai, W. J. Li, J. M. You, *Appl. Surf. Sci.* **2017**, 391, 592.
- [29] E. Longo, L. S. Cavalcante, D. P. Volanti, A. F. Gouveia, V. M. Longo, J. A. Varela, M. O. Orlandi, J. Andres, *Sci. Rep.* **2013**, 3, 1676.
- [30] J. Andres, L. Gracia, P. Gonzalez-Navarrete, V. M. Longo, W. Avansi, Jr, D. P. Volanti, M. M. Ferrer, P. S. Lemos, F. A. La Porta, A. C. Hernandez, E. Longo, *Sci. Rep.* **2014**, 4, 5391.
- [31] Y. V. B. De Santana, J. E. C. Gomes, L. Matos, G. H. Cruvinel, A. Perrin, C. Perrin, J. Andres, J. A. Varela, E. Longo, *Nanomater. Nanotechnol.* **2014**, 4, 22.

- [32] W. D. S. Pereira, J. Andres, L. Gracia, M. A. San-Miguel, E. Z. da Silva, E. Longo, V. M. Longo, *Phys. Chem. Chem. Phys.* **2015**, *17*, 5352.
- [33] M. A. San-Miguel, E. Z. da Silva, S. M. Zannetti, M. Cilense, M. T. Fabbro, L. Gracia, J. Andres, E. Longo, *Nanotechnology* **2016**, *27*, 225703.
- [34] Z. M. Xiu, Q. B. Zhang, H. L. Puppala, V. L. Colvin, P. J. J. Alvarez, *Nano Lett.* **2012**, *12*, 4271.
- [35] R. Yoksan, S. Chirachanchai, *Mater. Chem. Phys.* **2009**, *115*, 296.
- [36] V. M. Longo, C. C. De Foggi, M. M. Ferrer, A. F. Gouveia, R. S. Andre, W. Avansi, C. E. Vergani, A. L. Machado, J. Andres, L. S. Cavalcante, A. C. Hernandez, E. Longo, *J. Phys. Chem. A* **2014**, *118*, 5769.
- [37] T. George, S. Joseph, S. Mathew, *Pramana-J. Phys.* **2005**, *65*, 793.
- [38] M. Vafaezadeh, M. M. Hashemi, *Rsc Adv.* **2015**, *5*, 31298.
- [39] L. F. da Silva, A. C. Catto, W. Avansi, Jr, L. S. Cavalcante, J. Andres, K. Aguir, V. R. Mastelaro, E. Longo, *Nanoscale* **2014**, *6*, 4058.
- [40] L. S. Cavalcante, M. A. Almeida, W. Avansi, Jr, R. L. Tranquilin, E. Longo, N. C. Batista, V. R. Mastelaro, M. S. Li, *Inorg. Chem.* **2012**, *51*, 10675.
- [41] C.-X. Guo, B. Yu, J.-N. Xie, L.-N. He, *Green Chem.* **2015**, *17*, 474.
- [42] L. F. da Silva, A. C. Catto, W. Avansi, L. S. Cavalcante, V. R. Mastelaro, J. Andres, K. Aguir, E. Longo, *J. Alloys Compd.* **2016**, *683*, 186.
- [43] R. A. Roca, J. C. Sczancoski, I. C. Nogueira, M. T. Fabbro, H. C. Alves, L. Gracia, L. P. S. Santos, C. P. de Sousa, J. Andrés, G. E. Luz, Jr, E. Longo, L. S. Cavalcante, *Catal. Sci. Technol.* **2015**, *5*, 4091.
- [44] Z. Lin, J. Li, Z. Zheng, J. Yan, P. Liu, C. Wang, G. Yang, *Acs Nano* **2015**, *9*, 7256.
- [45] A. Sreedevi, K. P. Priyanka, S. R. Mary, E. M. Mohammed, T. Varghese, *Adv. Sci. Eng. Med.* **2015**, *7*, 498.
- [46] D. P. Dutta, A. Singh, A. Ballal, A. K. Tyagi, *Eur. J. Inorg. Chem.* **2014**, *2014*, 5724.
- [47] E. Longo, D. P. Volanti, V. M. Longo, L. Gracia, I. C. Nogueira, M. A. P. Almeida, A. N. Pinheiro, M. M. Ferrer, L. S. Cavalcante, J. Andres, *J. Phys. Chem. C* **2014**, *118*, 1229.
- [48] E. Longo, W. Avansi, J. Bettini, J. Andres, L. Gracia, *Sci. Rep.* **2016**, *6*, 21498.
- [49] A. Sreedevi, K. P. Priyanka, K. K. Babitha, S. Ganesh, T. Varghese, *Micron* **2016**, *88*, 1.
- [50] G. M. Faccin, M. A. San-Miguel, J. Andres, E. Longo, E. Z. da Silva, *J. Phys. Chem. C* **2017**, *121*, 7030.
- [51] R. Dovesi, V. R. Saunders, C. Roetti, R. Orlando, C. M. Zicovich-Wilson, F. Pascale, B. Civalieri, K. Doll, N. M. Harrison, I. J. Bush, P. D'Arco, M. Llunel, M. Causà, Y. Noël, *CRYSTAL14 User's Manual*, Theoretical Chemistry Group: University of Turin, Italy **2014**.
- [52] R. Dovesi, R. Orlando, B. Civalieri, C. Roetti, V. R. Saunders, C. M. Zicovich-Wilson, *Z. Kristallogr.* **2005**, *220*, 571.
- [53] A. D. Becke, *J. Chem. Phys.* **1993**, *98*, 5648.
- [54] C. T. Lee, W. T. Yang, R. G. Parr, *Phys. Rev. B* **1988**, *37*, 785.
- [55] F. Cora, A. Patel, N. M. Harrison, R. Dovesi, C. R. A. Catlow, *J. Am. Chem. Soc.* **1996**, *118*, 12174.
- [56] Crystal Basis Sets Library, [http://www.crystal.unito.it/Basis\\_Sets/Ptable.html](http://www.crystal.unito.it/Basis_Sets/Ptable.html)
- [57] G. Kresse, J. Hafner, *Phys. Rev. B* **1993**, *47*, 558.
- [58] G. Kresse, J. Furthmuller, *Comput. Mater. Sci.* **1996**, *6*, 15.
- [59] G. Kresse, J. Furthmuller, *Phys. Rev. B* **1996**, *54*, 11169.
- [60] H. J. Monkhorst, J. D. Pack, *Phys. Rev. B* **1976**, *13*, 5188.
- [61] P. E. Blochl, O. Jepsen, O. K. Andersen, *Phys. Rev. B* **1994**, *49*, 16223.
- [62] J. P. Perdew, J. A. Chevary, S. H. Vosko, K. A. Jackson, M. R. Pederson, D. J. Singh, C. Fiolhais, *Phys. Rev. B* **1992**, *46*, 6671.
- [63] J. P. Perdew, K. Burke, M. Ernzerhof, Generalized gradient approximation made simple. *Phys. Rev. Lett.* **1996**, *77*, 3865.
- [64] P. E. Blochl, *Phys. Rev. B* **1994**, *50*, 17953.
- [65] G. Kresse, D. Joubert, *Phys. Rev. B Condens. Matter Mater. Phys.* **1999**, *59*, 1758.
- [66] R. P. Feynman, *Phys. Rev.* **1939**, *56*, 340.
- [67] H. Jonsson, G. Mills, K. W. Jacobsen, B. J. Berne, *Classical and Quantum Dynamics in Condensed Phase Simulations*, World Scientific, Singapore **1998**.
- [68] R. F. W. Bader, *Atoms in Molecules: A Quantum Theory*, Clarendon Press Oxford, New York **1990**.
- [69] P. Hohenberg, W. Kohn, *Phys. Rev.* **1964**, *136*, B864.
- [70] P. L. A. Popelier, *Atoms in Molecules: An Introduction*, Prentice Hall, Harlow **2000**.
- [71] C. F. Matta, R. J. Boyd, *The Quantum Theory of Atoms in Molecules: From Solid State to DNA and Drug Design*, Wiley-VCH, Weinheim, Germany **2007**.
- [72] R. A. Roca, A. F. Gouveia, P. S. Lemos, L. Gracia, J. Andres, E. Longo, *Inorg. Chem.* **2016**, *55*, 8661.
- [73] J. Andres, M. M. Ferrer, L. Gracia, A. Beltran, V. M. Longo, G. H. Cruvinel, R. L. Tranquilin, E. Longo, *Part. Part. Syst. Char.* **2015**, *32*, 646.
- [74] G. Botelho, J. C. Sczancoski, J. Andres, L. Gracia, E. Longo, *J. Phys. Chem. C* **2015**, *119*, 6293.
- [75] S. Plimpton, *J. Comput. Phys.* **1995**, *117*, 1.
- [76] W. M. Brown, P. Wang, S. J. Plimpton, A. N. Tharrington, *Comput. Phys. Commun.* **2011**, *182*, 898.
- [77] W. M. Brown, A. Kohlmeyer, S. J. Plimpton, A. N. Tharrington, *Comput. Phys. Commun.* **2012**, *183*, 449.

- [78] W. M. Brown, M. Yamada, *Comput. Phys. Commun.* **2013**, *184*, 2785.
- [79] S. Nose, *Mol. Phys.* **1984**, *52*, 255.
- [80] S. Nose, *J. Chem. Phys.* **1984**, *81*, 511.
- [81] W. G. Hoover, *Phys. Rev. A* **1985**, *31*, 1695.
- [82] M. S. Daw, M. I. Baskes, *Phys. Rev. B* **1984**, *29*, 6443.
- [83] S. M. Foiles, M. I. Baskes, M. S. Daw, *Phys. Rev. B* **1986**, *33*, 7983.
- [84] R. A. Johnson, *Phys. Rev. B* **1989**, *39*, 12554.
- [85] Y. Mishin, D. Farkas, M. J. Mehl, D. A. Papaconstantopoulos, *Phys. Rev. B* **1999**, *59*, 3393.
- [86] H. W. Sheng, M. J. Kramer, A. Cadien, T. Fujita, M. W. Chen, *Phys. Rev. B* **2011**, *83*, 134118.
- [87] W. Humphrey, A. Dalke, K. Schulten, *J. Mol. Graph.* **1996**, *14*, 33.
- [88] A. Varshney, F. P. Brooks, W. V. Wright, *IEEE Comput. Graph. Appl.* **1994**, *14*, 19.
- [89] A. Stukowski, *Modell. Simul. Mater. Sci. Eng.* **2010**, *18*, 015012.
- [90] J. D. Honeycutt, H. C. Andersen, *J. Phys. Chem.* **1987**, *91*, 4950.
- [91] A. J. van den Berg, C. A. H. Juffermans, *J. Appl. Crystallogr.* **1982**, *15*, 114.
- [92] X. F. Chang, S. B. Wang, Q. Qi, M. A. Gondal, S. G. Rashid, S. Gao, D. Y. Yang, K. Shen, Q. Y. Xu, P. Wang, *Dalton Trans.* **2015**, *44*, 15888.
- [93] Y. Yu, C. Y. Cao, H. Liu, P. Li, F. F. Wei, Y. Jiang, W. G. Song, *J. Mater. Chem. A* **2014**, *2*, 1677.
- [94] S. Sepulveda-Guzman, N. Elizondo-Villarreal, D. F. A. Torres-Castro, X. Gao, J. P. Zhou, M. Jose-Yacamán, *Nanotechnology* **2007**, *18*, 335604.
- [95] D. S. Su, M. Wieske, E. Beckmann, A. Blume, G. Mestl, R. Schlogl, *Catal. Lett.* **2001**, *75*, 81.
- [96] Z. Q. Liu, H. Hashimoto, E. Sukei, M. Song, K. Mitsuishi, K. Furuya, *Phys. Rev. Lett.* **2003**, *90*, 255504.
- [97] A. L. Koh, K. Bao, I. Khan, W. E. Smith, G. Kothleitner, P. Nordlander, S. A. Maier, D. W. McComb, *Acs Nano* **2009**, *3*, 3015.

#### AUTHOR BIOGRAPHIES



**JUAN ANDRÉS** is Full Professor of Physical Chemistry at the Universitat Jaume I, and Director of Theoretical and Computational Chemistry Group and completed his Ph.D. degree in Physical Chemistry at Universitat of Valencia, Spain, under the supervision of Prof. E. Silla in 1984. He undertook postdoctoral studies at Uppsala Universitet, in Sweden, with Prof. Orlando Tapia. Prof. Andrés was invited Professor at the Université Pierre et Marie Curie (Paris, France) working with Prof. B. Silvi; and at National Institute of Science and Technology of Materials in Nanotechnology, (Sao Carlos, Brazil) directed by Prof. E. Longo. His research interest covers a wide range of fields from structure and chemical reactivity, nanoscience and nanotechnology, materials science, and catalysis.



**AMANDA FERNANDES GOUVEIA** is a Ph.D. student in Inorganic Chemistry at the Federal University of São Carlos, under the supervision of Prof. E. Longo. She completed a sandwich period of her studies at the Universitat Jaume I, Spain, under the supervision of Prof. J. Andrés. Her research is in the field of theoretical and computational chemistry applied to solid states.



**LOURDES GRACIA** is Assistant Professor of Physical Chemistry at the University of Valencia. She received her Ph.D. in Physical Chemistry at the University Jaume I, under the supervision of Prof. J. Andrés and A. Beltrán in 2005. Her research is in the field of theoretical and computational chemistry, particularly the study of optical properties and mechanisms of nucleation and growth processes of metal filaments in perovskite ( $\text{ABO}_3$ ), scheelite ( $\text{ABO}_4$ ),  $\text{A}_2\text{O}_3$ ,  $\text{A}_2\text{BO}_4$  and  $\text{A}_3\text{BO}_4$  compounds based materials. In addition, theoretical studies of pressure-induced phase transitions in these compounds.



**ELSON LONGO** is Professor EMÉRITO of Federal University of São Carlos. He received his Ph.D. degree in Physical Chemistry at the Institute of Physics of University of São Paulo in São Carlos, under the supervision of Prof. R. C. Ferreira in 1984. He directed 74 theses and dissertations, 20 awards and honorable mentions. Partnership with national and international institutions of Spain (Juan Andres), France, USA and Italy. Director of CDMF/FAPESP. Member of the World Academy of Ceramics, ACIESP, and Brazilian Academy of Sciences.



**GIOVANI MANZEPI FACCIN** studied physics at the Universidade Estadual de Campinas (UNICAMP) in Brazil, where he received his Ph.D. in Physics in 2012. His research is in the field of applied theoretical methods and computational physics, covering applications in the areas of molecular dynamics, ab-initio calculations, finite element methods, applied heuristics and software development. Since 2015 he is a Professor Adjunto (analog to Associate Professor) at the Universidade Federal da Grande Dourados (UFGD), in Brazil.



**EDISON ZACARIAS DA SILVA** is Full Professor at the Institute of Physics Gleb Wataghin, State University of Campinas. Completed his Ph. D. in physics at Bristol University, UK, under the supervision of Balázs Györfy. Prof. da Silva was visiting scholar at Max Planck Institute in Stuttgart, Germany, Imperial College of Science, London and International Center for Theoretical Physics (ICTP), Trieste, Italy. His research interests are superconductivity, computer simulations, electronic structure of solids molecules, and nanostructures.



**DOUGLAS HENRIQUE PEREIRA** is Associate Professor of Physical Chemistry at the Federal University of Tocantins. He received his Ph.D. from the State University of Campinas, under the supervision of Prof. Rogério Custodio in 2013. Currently does postdoctoral studies at the State University of Campinas working with Prof. Miguel A. San-Miguel. His research is in the field of theoretical and computational chemistry, particularly implementation of pseudopotential in the Composite methods, theoretical studies of reaction mechanisms, and rotational barriers.



**MIGUEL ANGEL SAN-MIGUEL** is currently Professor in Physical Chemistry at the State University of Campinas (Brazil) since 2014. He completed his Ph.D. at the Universidad de Sevilla (1998) where worked as Professor in Physical Chemistry until 2014. He spent several post-doctoral stays at the Universities of Reading and Warwick (UK) with Prof. Mark Rodger, and was Visiting Professor at University of Oxford with Prof. Mark Sansom. His research interests include chemical reactivity, biomaterials, and catalysis.

## SUPPORTING INFORMATION

Additional Supporting Information may be found online in the supporting information tab for this article.

**How to cite this article:** Andrés J, Gouveia AF, Gracia L, et al. Formation of Ag nanoparticles under electron beam irradiation: Atomistic origins from first-principles calculations. *Int J Quantum Chem.* 2018;118:e25551. <https://doi.org/10.1002/qua.25551>